Journal of the Energy Institute

Differences in N species induced by pyrolysis temperature: d-band center adjustment over the biomass carbon-supported CoP for boosting hydrogen evolution reaction

--Manuscript Draft--

Manuscript Number:	JOTEI-D-23-01055
Article Type:	Research Paper
Keywords:	nitrogen species; electronic metal-support interactions; d-band center; work function; η10; hydrogen evolution reaction
Corresponding Author:	Dekui Shen Nanjing, Jiangsu CHINA
First Author:	Qichang Wang, Ph.D.
Order of Authors:	Qichang Wang, Ph.D.
	Jing Zhao, Doctor
	Ran Yu, Professor
	Dekui Shen, Professor
	Chunfei Wu, Doctor
	Kai Hong Luo, Professor
Manuscript Region of Origin:	Asia Pacific
Abstract:	Nitrogen (N) species in biomass-based carbon can be adjusted through pyrolysis at different temperatures, optimizing the valence band structure of supported metal nanoparticles through electronic metal-support interactions (EMSIs). Herein, ginkgo leaves-based carbon supported cobalt phosphide (CoP@NSPC-T, T =850, 900 and 950 oC) was obtained via carbothermal reduction method at different pyrolysis temperature. Pyridinic N and pyrrolic N in carbon lattice were dramatically decreased with pyrolysis temperature raised, whereas the graphitic N showed the opposite trend. The change in N species (pyridinic N, pyrrolic N and graphitic N) reconfigured the valence band structure of CoP@NSPC-T, inducing the enhancement of work function and the upshift of d-band center. A relationship between the ratio of (pyridinic N + pyrrolic N)/graphitic N, work function, d-band center, and HER activity (η10) of catalysts was established. CoP@NSPC-900 with a moderate work function value and d-band center tend to achieve a balance for Volmer process and Heyrovsky process, exhibiting the lowest η10 value activity among the resulted catalysts as the ratio of (pyridinic N + pyrrolic N)/graphitic N is 1.33.
Suggested Reviewers:	Zhaofu Fei, Doctor Scientist, Federal Polytechnic School of Lausanne zhaofu.fei@epfl.ch We suggest Dr. ZhaoFu Fei to be reviewer for our manuscript in that he has rich experience in the organic chemistry synthesis and analysis.
	Lianhua Xu, Doctor Zhejiang University xulianhua@zju.edu.cn Doctor Xu has deep insights in preparation of design and synthesis of cobalt-based phosphide electrocatalysts.
	Guixiang Li, Doctor guixiang.li@uni-bielefeld.de Dr. Li is very good at the synthesis of biomass-based hydrogen evolution electrocatalysts.
	Chanatip Samart, Doctor Thammasat University chanatip@tu.ac.th We suggest Dr. Samart Chanatip to be reviewer for our manuscript in that he has deep

	insight into the research on conversion of biomass.
Opposed Reviewers:	

Journal of the Energy Institute

Cover letter

Dear editor:

I, on behalf of all authors, hereby submit the manuscript entitled "*Differences in N species induced by pyrolysis temperature: d-band center adjustment over the biomass carbon-supported CoP for boosting hydrogen evolution reaction"* for consideration as an article in ***Journal of the Energy Institute***.

Tuning the nitrogen (N) species (pyridinic N, pyrrolic N and graphitic N) in carbon support has been demonstrated to be an efficient way to tailor the valence band structure for supported metal nanoparticles via the electronics metal-support interactions (EMSIs). To optimize the valence band-structure of supported CoP nanoparticles, we were attracted to establish the relationship between the ratio of (pyridinic N + pyrrolic N)/graphitic N, work function, and HER activity.

In this work, ginkgo leaves-based carbon supported CoP with differ N species were prepared at 850, 900 and 950 ^{o}C (CoP@NSPC-850, CoP@NSPC-900, and CoP@NSPC-950). We conducted an in-depth analysis of the impact of N species on the d-band center and work function for CoP through XPS, UPS, and electrochemical measurements. As the pyrolysis temperature increased, the content of pyridinic N and pyrrolic N decreased, while the graphitic N content showed an opposite trend, resulting in a reconfiguration of the valence band structure. This reconfiguration led to an upshift

of the d-band center towards the Fermi level, as well as an increase in the work function value. When the ratio of (pyridinic N + pyrrolic N)/graphitic N was 1.33, the d-band center and work function were optimized, resulting in a balance between the Volmer process and Heyrovsky process, and ultimately leading to the best HER activity for CoP@NSPC-900.

This work provides new insights in catalysts design through establishing the relationship between its chemical properties, valence band structure and catalytic activity, which is valuable for large-scale preparation of electrocatalysts from raw biomass.

I sincerely appreciate you for reviewing the manuscript and considering the publication of this work. Look forward to your positive feedback. Thanks a lot!

Yours sincerely,

Prof. Dekui Shen

Key Laboratory of Thermal Conversion and Control, Ministry of China

School of Energy and Environment, Southeast University

E-mail: 101011398@seu.edu.cn (D. K. Shen)

Highlights

1 Nitrogen species in biomass derived carbon support is tuning by adjusting the pyrolysis temperature.

2 The impact of differ nitrogen species on the d-band center of CoP has been in-depth studied.

3 A relationship between nitrogen species, d-band center, work function and catalytic activity is finally established.

Graphical Abstract

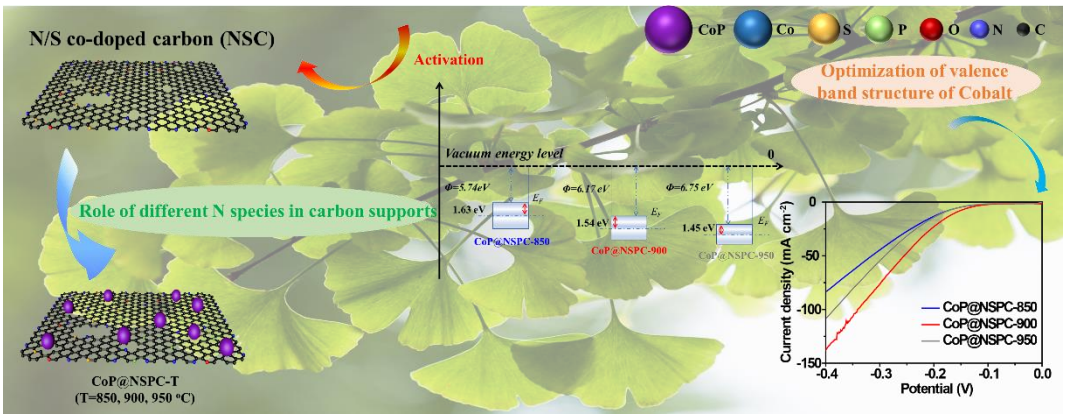

Differences in N species induced by pyrolysis temperature: d-band center adjustment over the biomass carbon-supported CoP for boosting hydrogen evolution reaction

Qichang Wang[a], Jing Zhao[a], Ran Yu[a], Dekui Shen[a#], Chunfei Wu[c], Kai Hong Luo[d]

[a] Key Laboratory of Energy Thermal Conversion and Control of Ministry of Education, School of Energy and Environment, Southeast University, Nanjing 210096, Jiangsu, PR China

[b] School of Chemistry and Chemical Engineering, Queen's University Belfast, Belfast, BT7 1NN, United Kingdom

[c] Department of Mechanical Engineering, University College London, London, WC1E 7JE, United Kingdom

* Corresponding author: * 101011398@seu.edu.cn (D. K. Shen)

Abstract: Nitrogen (N) species in biomass-based carbon can be adjusted through pyrolysis at different temperatures, optimizing the valence band structure of supported metal nanoparticles through electronic metal-support interactions (EMSIs). Herein, ginkgo leaves-based carbon supported cobalt phosphide (CoP@NSPC-T, T =850, 900 and 950 ^{o}C) was obtained via carbothermal reduction method at different pyrolysis temperature. Pyridinic N and pyrrolic N in carbon lattice were dramatically decreased with pyrolysis temperature raised, whereas the graphitic N showed the opposite trend.

The change in N species (pyridinic N, pyrrolic N and graphitic N) reconfigured the valence band structure of CoP@NSPC-T, inducing the enhancement of work function and the upshift of d-band center. A relationship between the ratio of (pyridinic N + pyrrolic N)/graphitic N, work function, d-band center, and HER activity (η_{10}) of catalysts was established. CoP@NSPC-900 with a moderate work function value and d-band center tend to achieve a balance for Volmer process and Heyrovsky process, exhibiting the lowest η_{10} value activity among the resulted catalysts as the ratio of (pyridinic N + pyrrolic N)/graphitic N is 1.33.

Key words: nitrogen species, electronic metal-support interactions, d-band center, work function, η_{10}, hydrogen evolution reaction.

1 Introduction

High consumption of fossil fuel leads to a serious energy crisis and environment pollution. [1, 2] Searching alternative energy is urgent to relief these problems. Hydrogen gas (H_2) is an ideal clean energy carrier with high energy density (142 MJ kg^{-1}), and has attracted more attentions. [3-6] In contrast of the traditional H_2 production method, electrocatalytic water splitting integrated with clean energy (solar, wind energy, etc.) provides a cost-effective and environment-friendly way for large scale H_2 production. [7-9] However, noble metal (Pt, Ir, etc.) derived catalyst is regarded as the most efficient catalyst for hydrogen evolution reaction (HER), but the high-cost and low-abundance still restricts its practical application. [10, 11] Hence, developing

efficient and cheap HER electrocatalysts is essential to consummate the roadmap of hydrogen economy.

Recently, differ non-noble metal-based electrocatalysts have been investigated to catalytic HER process, such as transition metal sulfides, carbides, phosphides. [12-18] Among these catalysts, transition metal phosphides (TMPs) have stood out due to their excellent catalytic activity, acid compatibility and economic practicality. [1, 19-22] Cobalt phosphide (CoP) is one of such appealing catalysts for the HER, and has been extensively studied. [23, 24] While most CoP-based catalysts will meet the problems of agglomeration during the pyrolysis process, which can be addressed by using a support to anchor the CoP nanoparticles (NPs) and increase the dispersion of CoP NPs via electronic metal-support interactions (EMSIs). [1, 25] The highly delocalized charge density in metal atoms caused by the EMSIs can be used to reconstruct the d-band structure and alter the charge transfer between the metal atoms and carbon substrates. [26] A faster kinetic process for HER will come from the reconfiguration of the d-band structure, which ascribes from the optimization of the binding energy between catalysts and intermediates (H*, H_2).

To date, several studies have been devoted to focusing on tuning the d-band structure of supported metal nanoparticles by adjusting the properties of heteroatoms in the supports. [27, 28] [29, 30] For instance, Lie et al. altered the electronic structure of the active sites of Co-Ag dual metal sites by introducing P doping in carbon nitride,

inducing an optimize of valence band structure, promoting its photocatalytic hydrogen production properties. [29] Lu et al. demonstrated that the high HER activity of ruthenium and nitrogen co-doped carbon nanowires stemmed from the formation of Ru centers linked to the coordination of N and C, resulting in a lower hydrogen binding energy compared to the catalyst without N doping.[31] Ning and co-works investigated the electronic effects of different N species interacting with Pt and found that pyridinic N acted as an electron acceptor, whereas graphitic N functioned as an electron donor for the Pt nanoparticles. The presence of different N species in carbon nanotube led to distinct d-band structures of loaded Pt particles.[32] Thereby, efficiently tailoring the d-band structure of supported metal can be accomplished by adjusting the hetero dopants in supports, resulting in an optimized binding energy between catalysts and reaction intermediates.

Biomass derived porous carbon is a potential sustainable support due to its adjustable physical-chemistry properties, which is also regarded as a method for adequate valorization of biomass. [33-41] Natural organic elements (e.g., N) will be introduced into the carbon lattice as dopants, enabling the fine-tuning of the valence band structure of supported TMP NPs through the EMSIs. [42, 43] Additionally, dopants can be adjusted within the pyrolysis temperature, resulting different types of dopants in carbon lattice and unique electronic structures that modify the interactions between carbon supports and CoP, thus cause different catalytic properties. [44, 45] Therefore, we prepared ginkgo leaves based-carbon supported CoP by carbothermal reduction method,

and adjusted the heteroatom species in the supports by changing the reaction temperature. The natural dopants (N and S) in carbon lattice were analyzed through X-ray photoelectron spectroscopy (XPS) study. Given that the atomic ratio of S in carbon supports is below 0.28 at%, no significant changes in S dopants were detected in the supports, thus the changing of S dopants can be disregarded for the present analysis. While the N dopants in carbon lattice have relative higher proportion (> 2.8 at%), and various N species exhibit noticeable regular changes with increasing pyrolysis temperature. In contrast, the change of the introduced P component lacks any apparent regularity. (see below analysis). Hence, we prioritize N as the primary factor of interest to investigate its influence on the d-band center position of the resulting catalysts. The d-band center of resulting catalysts was then obtained through ultraviolet photo-electron spectroscopy (UPS). With further investigation of HER activity of CoP@NSC-T (T=850, 900 and 950 ^{o}C), the relationship between N species, d-band center of CoP, and catalytic activity was finally established. At 900 ^{o}C, a moderate ratio of different N species was achieved, with the ratio of (pyridinic N + pyrrolic N)/graphitic N being 1.33, enabling CoP@NSPC-900 to exhibit the most effective catalytic performance among the resulting catalysts.

2 Materials and methods

2.1 Chemical reagents

Sinopharm Chemical Reagent Co., Ltd. supplied the cobalt (II) nitrate hexahydrate ($Co(NO_3)_2 \cdot 6H_2O$, 99.99%), zinc chloride hexahydrate ($ZnCl_2 \cdot 6H_2O$, 99.99%),

magnesium chloride hexahydrate ($MgCl_2 \cdot 6H_2O$, 99.99%), 2-methylimidazole (2-MeIm), and phytic acid (PA, 55–70 wt.%), which were used without further purification.

Ginkgo leaves were collected from trees during autumn in Nanjing, Jiangsu Province, China. The collected leaves were washed with ultrapure water and dried in an oven at 80°C for 12 hours. Then, they were crushed using a pulverizer to obtain ginkgo leaf powders.

2.2 Preparation of nitrogen/sulfur co-doped carbon supported cobalt phosphide (CoP@NSPC-T)

The synthesize procedure was based on our previous work. [46] N and S co-doped carbon (NSC) was obtained via a simple carbonization protocol using the $ZnCl_2$ and $MgCl_2$ as the activators. The $Co(NO_3)_2 \cdot 6H_2O$ (30 mg) and 2-MeIm (42 mg) were dissolved in 5 ml ultra-pure water and stirred to form blue suspension. Phytic acid (250 μL) was then pour into the blue suspension to obtain a pink solution. Subsequently, NSC powders (120 mg) was dispersed homogenous in 10 ml ultra-pure water and mixed with afore-mentioned pink solution. The mixture was vigorously stirred for 6 h and evaporated using a water bath at 60 ^{o}C, and further dried at 80 ^{o}C under vacuum. To identify the effect of the dopants of NSC on the d-band center of supported Co compounds, the pyrolysis process was conducted at different temperature. Since our previous work [46] has demonstrated that the resulting catalyst obtained at 800 and 900 ^{o}C did not correspond to the crystal of CoP and exhibited low HER activity, the

pyrolysis temperatures in this study were set at 850, 900 and 950 ^{o}C to adjust the dopant type in carbon lattice. The resulted catalysts were denoted as CoP@NSPC-T (T = 850, 900 and 950).

2.3 Characterization of the prepared materials

The morphology of the CoP@NSPC-T was examined via scanning electron microscopy (SEM) and transmission electron microscopy (TEM) on the FEI quanta 400FEG and FEI Tacnai 20 electron microscope, respectively. The X-ray powder diffraction (XRD) was conducted on Bruker D8 to study the crystal structure of catalysts. The K-Alpha X-ray photoelectron spectroscopy (XPS) was taken on a Thermo ESCALAB 250XI to identify the element chemical states on materials surface, with the binding energy was calibrated using C1s at 284.6 eV. Raman spectra was recorded on an iHR550 Raman microscope (HOR-IBA scientific) at a range of 400~4000 cm^{-1}. To obtain the work function (Φ) of CoP@NSPC-T, ultraviolet electron spectroscopy (UPS) was performed using a Phi5000 VersaProbeIII with a bias voltage of -10 V. Besides, the position of d-band center was identified from the raw UPS spectrum.

2.4 Electrochemical experiment setup

A conventional three-electrode system was used to study the HER performance of CoP@NSPC-T. The electrocatalytic measurements for HER was conducted on CHI 760E electrochemical workstation at ambient condition with N_2 saturation. in 0.5 M H_2SO_4. The graphite rod was selected as the counter electrode. The mercury/mercurous

sulfate electrode (Hg/Hg_2SO_4) served as the reference electrode. The glass carbon electrode (GC, 0.196 cm^{-2}) modified with catalysts ink was used as the working electrode. Such catalysts ink was prepared by mixing the 10 mg of the CoP@NSPC-T with 1000 μL ethanol/deionized water (V:V = 1:3) and sonicated for 30 mins. The well-mixed catalysts ink (10 μL) was dropped onto the GC and dried naturally. Subsequently, the Nafion (5 wt.%, 10 μL) was dropped onto the GC to keep the catalyst steady on the surface of GC. The linear sweep voltammetry (LCV) plots were recorded with a scan rate of 2 mV s^{-1}. The double layer capacitance (C_{dl}) associated with the electrochemical surface area (ECSA) was evaluated through the cyclic voltammetry (CV) tests at a range of -0.5~-0.3 V with a scan rate of 10, 30, 50, 70, 90 mV s^{-1}, respectively. All the HER testes were taken IR-correct and the obtained potentials were converted to a reversible hydrogen electrode (RHE) using the equation of $E_{vs.RHE} = E_{vs}Hg/Hg_2SO_4 + E^{\theta}Hg/Hg_2SO_4 + 0.059$ pH, where $E^{\theta}Hg/Hg_2SO_4$ was equal to 0.697 V.

3 Results and discussion

3.1 Characteristic of CoP@NSPC-T

The N/S co-doped carbon supported CoP (CoP@NSPC) was prepared via a carbothermal reduction method, following our previous work, [46] which is illustrated schematically in Scheme 1. Ginkgo leaf powder served as the C, N and S sources was firstly activated using $ZnCl_2$ and $MgCl_2$ during the carbonization process at 750 ^{o}C under N_2 protection, and the resulting products was further washed with 3 M HCl, leaving behind N/S co-doped carbon (NSC). The activation process significantly

altered the sheet-like morphology of raw ginkgo leaf powders (Figure S1), leading to the formation of numerous pores (Figure 1a) which will benefit to its mass and electronic transfer. Subsequently, NSC, ZIF-67, and PA were sequentially mixed, water bathed, and dried to obtain the precursor. The dry precursor was then pyrolyzed at 850, 900 and 950 ^{o}C under N_2 atmosphere, and the resulting catalysts were named CoP@NSPC-850, CoP@NSPC-900 and CoP@NSPC-950, respectively.

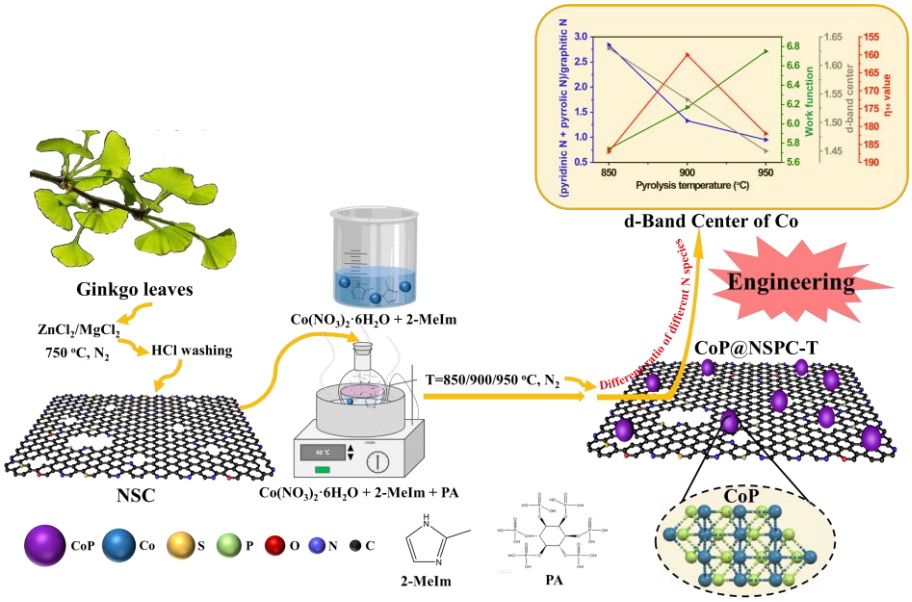

Scheme 1 Schematic illustration of preparation of CoP@NSC-T (T = 850, 900 and 950 ^{o}C).

The morphology and structure of the resulting catalysts were then extensively characterized through HRTEM and HAADF-STEM measurements. The HRTEM images unveiled intriguing details, including a fringe spacing of 2.79 Å, suggesting the possible presence of well-defined (002) lattice planes of CoP, whereas the surrounding amorphous region was speculated to be the ginkgo leaves-based carbon supports

(Figure 1b). These observations provided the evidence to support the structure of carbon supported CoP. Furthermore, HAADF-STEM revealed that the highly dispersed light flake CoP particles throughout the entire carbon supports (Figure 1c), corroborating the findings from HRTEM. The EDS elemental mapping validated the presence of C, N, O, S, and P, distributed across the entirety of the obtained materials (Figure 1d). Co is predominantly dispersed in the form of nanoparticles, namely CoP, as evidenced by the enrichment of P in the areas where Co accumulates. An enrichment of O around Co element was proposed to result from the slightly oxidized P and Co states due to the inevitable surface oxidation upon exposure to air. Notably, although the distribution of S is also enriched along with Co, we hypothesize that S primarily exists as the dopants in carbon lattice. A comprehensive analysis was provided in the XRD and XPS sections for further insights and understanding.

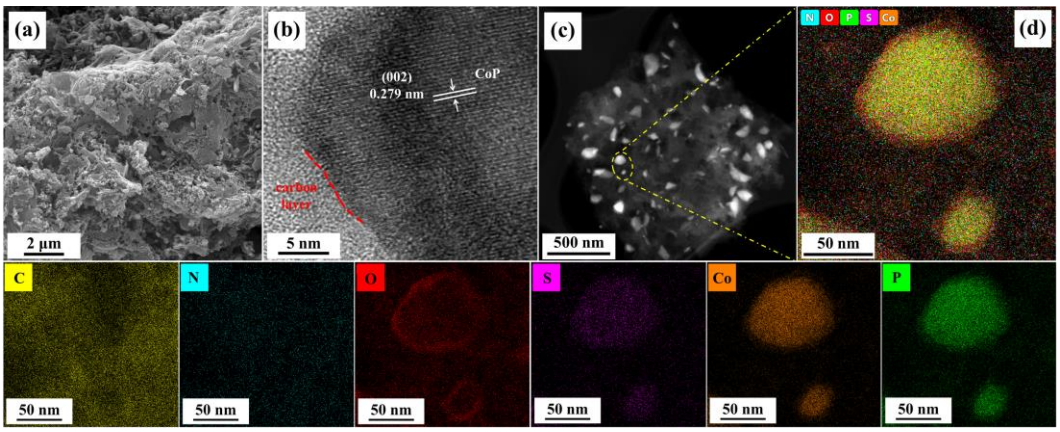

Figure 1 (a) SEM, (b) HRTEM, (c) HAADF-STEM images and (e) EDS elemental mapping images of CoP@NSPC-900.

The XRD measurement was employed to study the structure of resulting catalysts

within different pyrolysis temperature (Figure 2a). CoP@NSC-850, CoP@NSPC-900 and CoP@NSPC-950 exhibited same diffractions (Figure 2a). The peaks centering at 32 °, 36 °, 46 °, 48 °, 52 °, and 57 ° indicates the (011), (002), (200), (111), (102), (210), (112), (211), (103), (020) and (212) planes of CoP (JCPDS-29-0497). From Raman spectrum, there are two distinct peaks locating at ~1350 cm^{-1} and ~1580 cm^{-1}, representing the disordered carbon (D band) and graphite carbon (G band), respectively (Figure 2b). The ratio of the intensity of D band and G band (I_D/I_G) represents the graphitization degree for the carbon support. [47, 48] The value of I_D/I_G for CoP@NSPC-850, CoP@NSPC-900 and CoP@NSPC-950 is 1.08, 1.05 and 1.00, respectively (Figure 2b). The decreased value of I_D/I_G verifies the increased graphitization degree as the pyrolysis temperature was raised.

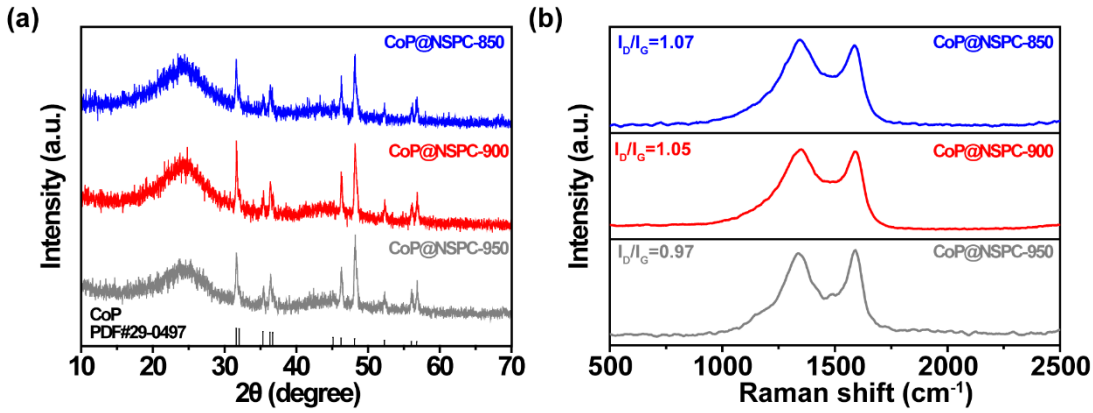

Figure 2 (a) XRD patterns, (b) Raman spectrum of CoP@NSPC-T (T=850, 900, 950 °C)

The chemical states of different elements on the catalysts' surface were analyzed via XPS study (Figure 3a and S3-5). The detailed amounts for Co, P, S and N species were

further calculated using the integral area (Table S1-4). All the peaks of Co, P, S and N in fine spectrum of CoP@NSPC-850, CoP@NSPC-900 and CoP@NSPC-950 were found to be at comparable binding energies in similar structures (Figure 3a and S2-4). The high-resolution Co 2p spectrum depicts four peaks centering at 798.09, 781.93, 803.58 and 786.99 eV, namely Co $2p_{1/2}$, Co $2p_{3/2}$ and Co oxidations states (Figure S2a, 3a and 4a). The change in pyrolysis temperature has not caused a substantial impact on the contents of differ Co species (Table S1). There are four peaks located at 134.36, 132.98, 130.15 and 129.71 in the high-resolution P 2p spectrum, indicating to the P-O, P-C, P $2p_{1/2}$ and P $2p_{3/2}$ (Figure S2b, 3b and 4b). As shown in Table S2, the quantities of P $2p_{1/2}$ and P $2p_{3/2}$, indicating the bonding between Co and P, remain essentially unchanged, while the variations in the content of P-C and P-O components show random behavior. To achieve complete conversion of Co into CoP, an excessive amount of PA was introduced during the precursor treatment, which cause the basically identical content of P $2p_{1/2}$ and P $2p_{3/2}$ observed for CoP@NSPC-850, CoP@NSPC-900, and CoP@NSPC-950. Due to its colloidal properties, PA is susceptible to adhere to the beaker wall, thus making some loss during the precursor treatment, which could explain the fluctuations in P-O and P-C contents. High-resolution S 2p spectrum of resulting catalysts can be divided into three peaks located on the 163.79 eV, 164.89 eV and 169.19 eV, corresponding to the presence of S-C-S, C=S and C-SO_x-C, respectively (Figure S2c, 3c and 4c). The total atomic ratio of S atoms for CoP@NSPC-T (T = 850, 900 and 950 ^{o}C) is generally lower than 0.28 at%, thus the slight change of various S species was ignored (Table S3). The high-resolution N 1s spectrum of all resulting

CoP@NSPC-T was subdivided into four peaks centering at 400.8, 398.45, 402.08, and 399.78 eV, indicating the pyrrolic N, pyridinic N, graphitic N and Co-N, respectively (Figure 3a).

The amounts of Co-N are basically constant, while the contents of other N species undergo significant change as the pyrolysis temperature increases (Table S4). The relative atomic ratio of pyridinic N and pyrrolic N decreases with the increase in pyrolysis temperature. Conversely, the content of graphitic N increases with the rise in pyrolysis temperature, corresponding to the increased graphitic degree shown in Raman results (Figure 2b). The variations in pyridinic nitrogen, pyrrolic nitrogen, and graphitic nitrogen in carbon supports exhibit an obvious dependence on temperature. Pyridinic N and pyrrolic N are generally considered as the active sites for HER, while graphitic N often provides a good conductivity for carbon materials. [49, 50] The alteration of nitrogen content in the carbon support could potentially be the crucial factor influencing the activity of resulting catalyst. Therefore, different ratio of N species can tailor the band structure through the EMSIs, thus affecting the binding energy with various intermediates. [50] UPS measurements was further conducted to study the work function and d-band center of CoP@NSPC-850, CoP@NSPC-900, and CoP@NSPC-950 (Figure S5-8).

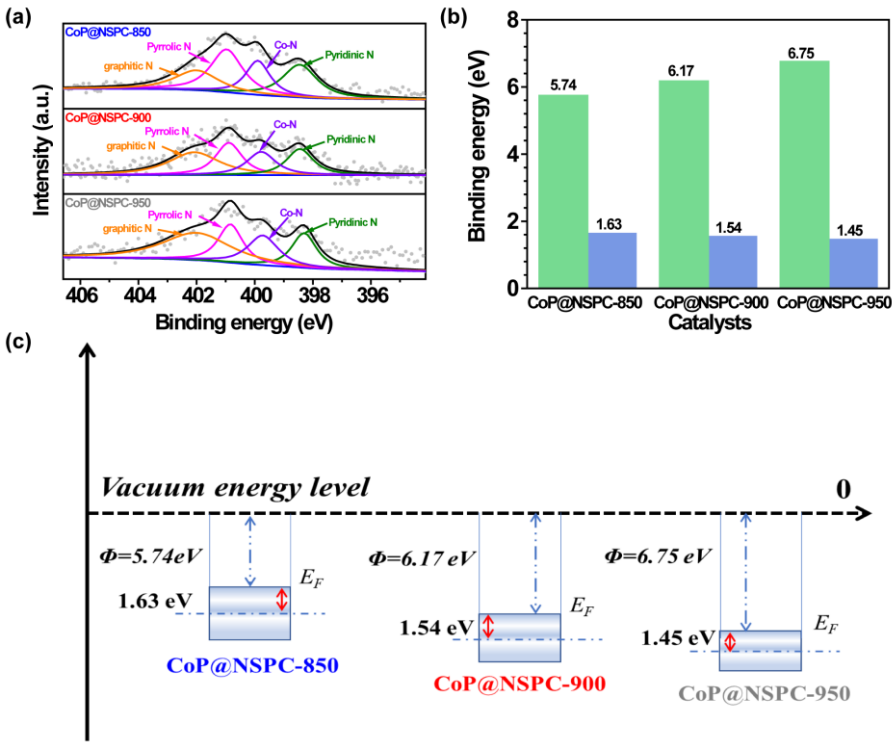

Figure 3 (a) N 1s and (b) value of work function (green) and d-band center (blue) for CoP@NSPC-T (T = 850, 900 and 950 ^{o}C), (c) schematic illustration of valence band structure of CoP@NSPC-T (T = 850, 900 and 950 ^{o}C).

The work function was firstly determined from the UPS spectrum with -10 V bias (Figure S5a). The secondary electron cut-off edge for CoP@NSPC-850, CoP@NSPC-900, and CoP@NSPC-950 was measured to be 15.48, 15.05, and 14.47 eV (Figure S5b), respectively. The value of work function (Φ) for CoP@NSPC-850, CoP@NSPC-900, and CoP@NSPC-950 was calculated to be 5.74, 6.17, and 6.75 eV (Figure 3b), respectively. The value of Φ indicates the ability for electron capturing. [51, 52] The position of the d-band center, which serves as a descriptor of hydrogen binding energy, was then resolved within the raw UPS spectrum (Figure S6a, 7a and 8a). The linear intersection near the Fermi level depicted the d-band center of CoP@NSPC-850,

CoP@NSPC-900, and CoP@NSPC-950, which locates at 1.63, 1.54, and 1.47 eV (Figure 3b and S6b, 7b, 8b). As a result, we can construct a schematic diagram representing the valence band spectrum of the resulting CoP@NSPC-850, CoP@NSPC-900 and CoP@NSPC-950 (Figure 3c). To obtain the most active catalysts for HER, the hydrogen binding energy should be moderate to maintain a balance between the adsorption and desorption process with reaction intermediates during HER. Thereby, the HER activity of CoP@NSPC-850, CoP@NSPC-900, and CoP@NSPC-950 have been in-depth studied using electrochemical experiment to determine the best catalysts among CoP@NSPC-T (T=850, 900 and 950 ^{o}C).

3.2 HER performance of CoP@NSPC-T

The IR-compensated LSV curves were recorded in N_2 saturated 0.5 M H_2SO_4 to evaluate the HER performance of CoP@NSPC-T and 20% Pt/C (Figure 4a). It is obviously that the 20% Pt/C exhibits best HER activity. CoP@NSPC-900 shows better performance than CoP@NSPC-850 and CoP@NSPC-950, while the η_{10} value for CoP@NSPC-850, CoP@NSPC-900 and CoP@NSPC-950 are 187, 160 and 182 mV, respectively. The corresponding Tafel plots for CoP@NSPC-850, CoP@NSPC-900 and CoP@NSPC-950 are 105.8, 87.5 and 97.0 mV dec^{-1} (Figure 4b). In term of the ideal Tafel slopes of 29, 38 and 116 mV dec^{-1} corresponding to different rate-determining steps of HER, [53] the electrocatalytic reaction on the surface of CoP@NSPC-850, CoP@NSPC-900 and CoP@NSPC-950 follows the Volmer–Heyrovsky mechanism. The lowest Tafel slope of CoP@NSPC-900 suggests a faster kinetic process compared

with CoP@NSPC-850 and CoP@NSPC-950. [54] The electrochemical surface area was accessed using double-layer capacitor (C_{dl}), which is determined from cyclic voltammetry (CV) with different scan rates (Figure S9). The fitted C_{dl} of CoP@NSPC-850, CoP@NSPC-900 and CoP@NSPC-950 is 60.4 109.4 and 63.2 mF cm^{-2}, respectively (Figure 4c), indicating there are more accessible active sites in CoP@NSPC-900. In addition, long term stability test of catalytic activity was also conducted via chronoamperometric response (i-t) tests, which have been already proved in our previous work. [46]

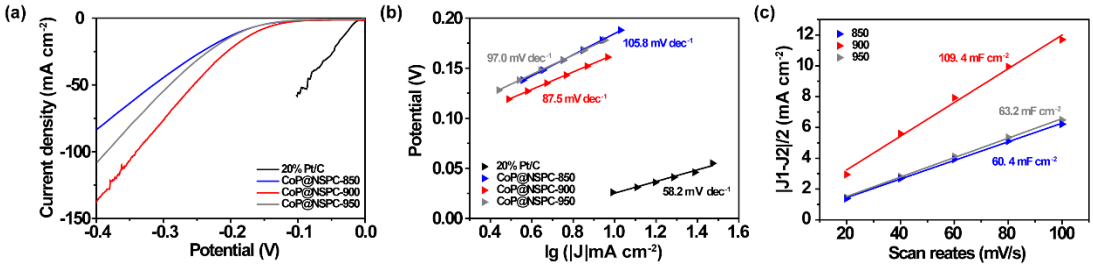

Figure 4 (a) recorded LSV curves () and (b) corresponding Tafel plots of CoP@NSPC-T (T = 850, 900 and 950 °C) and 20% Pt/C and (c) C_{dl} stands for CoP@NSPC-T (T = 850, 900 and 950 °C)

3.3 Mechanism analysis for the process

According to the electrochemical experiments, it is observed that the HER process on the surface of CoP@NSPC-850, CoP@NSPC-900, and CoP@NSPC-950 follows the Volmer-Heyrovsky mechanism. During Volmer-process, hydrogen intermediates (H_{ads}) are formed on the catalysts surface by coupling the captured H^+ with electron on active sites. [1, 4] Subsequently, the H_{ads} combine with H^+ and electrons to form H_2 and release

from catalysts surface during the Heyrovsky process. [1] A balance between H_{ads} formation and H_2 desorption is crucial for accelerating the HER process. [50] Therefore, the relationship between the ratio of (pyridinic N + pyrrolic N)/graphitic N, work function, the position of d-band center, and η_{10} value have been established to analyze the detail HER process on the surface of CoP@NSPC-850, CoP@NSPC-900 and CoP@NSPC-950 ^{o}C (Figure 5).

The ratio of (pyridinic N + pyrrolic N)/graphitic N of CoP@NSPC-850, CoP@NSPC-900 and CoP@NSPC-950 ^{o}C is 2.84, 1.33 and 0.95, respectively (Figure 5). The gradually decreased ratio of (pyridinic N + pyrrolic N)/graphitic N reconfigures the valence band of resulting catalysts, inducing an enhancement of work function and an upshift of d-band center (Figure 3c). A higher value of work function is beneficial for electron capture, accelerating the Volmer process. [51, 52] On the other hand, the d-band center's shift towards the Fermi level will enlarge the desorption energy between H_2 and catalysts surface, slowing down the release of H_2. [55, 56] A binding energy that is neither too strong nor too weak between catalysts and reactants is favorable for the HER process. [19, 55, 56] As shown in Figure 5, CoP@NSPC-900 has an intermediate work function and d-band center, indicating the Volmer and Heyrovsky process occurring on the surface of CoP@NSPC-900 is more balanced compared to CoP@NSPC-850 and CoP@NSPC-950, thus result in a lowest η_{10} value of CoP@NSPC-900 among prepared catalysts (Figure 5).

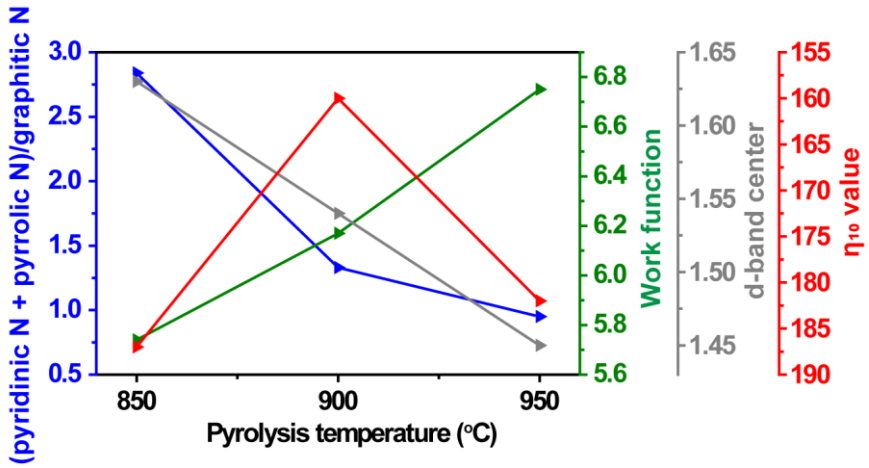

Figure 5 Relationship between the ratio of (pyridinic N + pyrrolic N)/graphitic N (blue), work function (green), the position of d-band center (grey), and η_{10} value (red) of resulting CoP@NSPC-T (850, 900 and 950 °C)

4 Conclusion

Carbon-supported CoP electrocatalysts were prepared using a carbothermal reduction method with ginkgo leaves as the carbon source. The ratio of different N species in carbon supports was adjusted through varying the pyrolysis temperature, leading an optimization of valence band structure of resulting CoP@NSPC-T (T = 850, 900 and 950 °C) by electronic metal-support interactions between carbon supports and CoP NPs. Based on the established relationship between the d-band center, work function, ratio of (pyridinic N + pyrrolic N)/graphitic N and η_{10} value of resulting catalysts, it was observed that the decrease of the ratio of (pyridinic N + pyrrolic N)/graphitic N resulted in the increase of work function and upshift of d-band center. The CoP@NSPC-900 catalyst, with a ratio of (pyridinic N + pyrrolic N)/graphitic N of 1.33, exhibited an optimal work function and d-band center, which kept a balance between Volmer and

Heyrovsky processes, resulting in the highest HER activity among the CoP@NSPC-T catalysts (T = 850, 900 and 950 ^{o}C). This study offers a new insight in designing an electrocatalyst by connecting their chemical properties, valence band structures, and catalytic activity, which could be valuable for the large-scale preparation of HER electrocatalysts.

Declaration of competing interest

The authors declare that they have no known competing financial interests or personal relationships that could have appeared to influence the work reported in this paper.

Acknowledgements

The authors gratefully acknowledge the support of the National Key Research and Development Plan of China (2020YFC1910000), Jiangsu Provincial Key Research and Development Program (BE2020114) and Chinese Scholarship Council (No. 202106090163).

Reference

[1] J. Zhu, L. Hu, P. Zhao, L.Y.S. Lee, K.Y. Wong, Recent Advances in Electrocatalytic Hydrogen Evolution Using Nanoparticles, Chem. Rev., 120 (2020) 851-918.

[2] B. Tian, W. Gao, X. Ning, Y. Wu, G. Lu, Enhancing water splitting activity by protecting hydrogen evolution activity site from poisoning of oxygen species, Appl. Catal., B, 249 (2019) 138-146.

[3] Z. Wan, S. Yang, G. Bao, J. Hu, H. Wang, Multiphase particle-in-cell simulation study of sorption enhanced steam methane reforming process in a bubbling fluidized bed reactor, Chem. Eng. J., 429 (2022) 132461.

[4] H. Pei, L. Zhang, G. Zhi, D. Kong, Y. Wang, S. Huang, J. Zang, T. Xu, H. Wang, X. Li, Rational construction of hierarchical porous FeP nanorod arrays encapsulated in polypyrrole for efficient and durable hydrogen evolution reaction, Chem. Eng. J., 433 (2022) 133643.

[5] L.-H. Xu, H.-B. Zeng, X.-J. Zhang, S. Cosnier, R.S. Marks, D. Shan, Highly active M2P2O7@NC (M = Co and Zn) for bifunctional electrocatalysts for ORR and HER, J. Catal., 377 (2019) 20-27.

[6] L.H. Xu, W.J. Wang, X.J. Zhang, S. Cosnier, R.S. Marks, D. Shan, Regulating the coordination capacity of ATMP using melamine: facile synthesis of cobalt phosphides as bifunctional electrocatalysts for the ORR and HER, Nanoscale, 14 (2022) 17995-18002.

[7] B. You, Y. Sun, Innovative Strategies for Electrocatalytic Water Splitting, Acc. Chem. Res., 51 (2018) 1571-1580.

[8] W.-H. Chen, C.-Y. Lu, W.-S. Chou, A. Kumar Sharma, A. Saravanakumar, K.-Q. Tran, Design and optimization of a crossflow tube reactor system for hydrogen production by combining ethanol steam reforming and water gas shift reaction, Fuel, 334 (2023) 126628.

[9] J. Hou, Y. Wu, B. Zhang, S. Cao, Z. Li, L. Sun, Rational Design of Nanoarray Architectures for Electrocatalytic Water Splitting, Adv. Funct. Mater., 29 (2019)

1808367.

[10] M. Yao, B. Wang, B. Sun, L. Luo, Y. Chen, J. Wang, N. Wang, S. Komarneni, X. Niu, W. Hu, Rational design of self-supported Cu@WC core-shell mesoporous nanowires for pH-universal hydrogen evolution reaction, Appl. Catal., B, 280 (2021) 119451.

[11] Y. Pan, K. Sun, Y. Lin, X. Cao, Y. Cheng, S. Liu, L. Zeng, W.-C. Cheong, D. Zhao, K. Wu, Z. Liu, Y. Liu, D. Wang, Q. Peng, C. Chen, Y. Li, Electronic structure and d-band center control engineering over M-doped CoP (M = Ni, Mn, Fe) hollow polyhedron frames for boosting hydrogen production, Nano Energy, 56 (2019) 411-419.

[12] J. Qu, Y. Li, F. Li, T. Li, X. Wang, Y. Yin, L. Ma, O.G. Schmidt, F. Zhu, Direct Thermal Enhancement of Hydrogen Evolution Reaction of On-Chip Monolayer $MoS_{(2)}$, ACS Nano, 16 (2022) 2921-2927.

[13] J. Wu, W. Zhong, C. Yang, W. Xu, R. Zhao, H. Xiang, Q. Zhang, X. Li, N. Yang, Sulfur-vacancy rich nonstoichiometric TiS_{2-x}/NiS heterostructures for superior universal hydrogen evolution, Appl. Catal., B, 310 (2022) 121332.

[14] X. Zhou, Y. Tian, J. Luo, B. Jin, Z. Wu, X. Ning, L. Zhan, X. Fan, T. Zhou, S. Zhang, X. Zhou, MoC Quantum Dots@N- Doped- Carbon for Low- Cost and Efficient Hydrogen Evolution Reaction: From Electrocatalysis to Photocatalysis, Adv. Funct. Mater., 32 (2022) 2201518.

[15] X. Fan, C. Liu, M. Wu, B. Gao, L. Zheng, Y. Zhang, H. Zhang, Q. Gao, X. Cao, Y. Tang, Synergistic effect of dual active sites over Ru/α-MoC for accelerating alkaline hydrogen evolution reaction, Appl. Catal., B, 318 (2022) 121867.

[16] J. Guo, C. Ouyang, Z. Zhan, T. Lei, P. Yin, Facile synthesis of tubular CoP as a high efficient electrocatalyst for pH-universal hydrogen evolution, Int. J. Hydrogen Energy, 47 (2022) 181-196.

[17] Z. Hu, X. Hao, Z. Jin, Morphology engineering ultrathin nitrogen-doped carbon Co-FeP derived from Co-Fe Prussian Blue Analogs for wide spectrum photocatalytic H_2 evolution, Fuel, 333 (2023) 126336.

[18] Y. Zheng, Y. Chen, X. Yue, S. Huang, Heteroatom Doping of Molybdenum Carbide Boosts pH-Universal Hydrogen Evolution Reaction, ACS Sustainable Chem. Eng., 8 (2020) 10284-10291.

[19] M. Gao, P. Gao, T. Lei, C. Ouyang, X. Wu, A. Wu, Y. Du, FeP/Ni2P nanosheet arrays as high-efficiency hydrogen evolution electrocatalysts, J. Mater. Chem. A, 10 (2022) 15569-15579.

[20] E. Vijayakumar, S. Ramakrishnan, C. Sathiskumar, D.J. Yoo, J. Balamurugan, H.S. Noh, D. Kwon, Y.H. Kim, H. Lee, MOF-derived CoP-nitrogen-doped carbon@NiFeP nanoflakes as an efficient and durable electrocatalyst with multiple catalytically active sites for OER, HER, ORR and rechargeable zinc-air batteries, Chem. Eng. J., 428 (2022) 131115.

[21] C. Wang, W. Li, X. Wang, N. Yu, H. Sun, B. Geng, Open N-doped carbon coated porous molybdenum phosphide nanorods for synergistic catalytic hydrogen evolution reaction, Nano Res., 15 (2021) 1824-1830.

[22] L.-H. Xu, P.-C. Che, X.-J. Zhang, S. Cosnier, D. Shan, FeP Nanoparticles Highly Dispersed on N,P-doped Petaloid Carbon Nanosheet: Interface Engineering and

Boosted Intrinsic ORR Activity, Appl. Surf. Sci., (2023) 156770.

[23] Y. Ren, Z. Li, B. Deng, C. Ye, L. Zhang, Y. Wang, T. Li, Q. Liu, G. Cui, A.M. Asiri, Y. Luo, X. Sun, Superior hydrogen evolution electrocatalysis enabled by CoP nanowire array on graphite felt, Int. J. Hydrogen Energy, 47 (2022) 3580-3586.

[24] X. Yang, A.-Y. Lu, Y. Zhu, M.N. Hedhili, S. Min, K.-W. Huang, Y. Han, L.-J. Li, CoP nanosheet assembly grown on carbon cloth: A highly efficient electrocatalyst for hydrogen generation, Nano Energy, 15 (2015) 634-641.

[25] Q. Guan, W. Li, A novel synthetic approach to synthesizing bulk and supported metal phosphides, J. Catal., 271 (2010) 413-415.

[26] M. Xie, F. Dai, J. Li, X. Dang, J. Guo, W. Lv, Z. Zhang, X. Lu, Tailoring the Electronic Metal-Support Interactions in Supported Atomically Dispersed Gold Catalysts for Efficient Fenton-like Reaction, Angew Chem. Int. Ed., 60 (2021) 14370-14375.

[27] Z. Chen, L. Liang, H. Yuan, H. Liu, P. Wu, M. Fu, J. Wu, P. Chen, Y. Qiu, D. Ye, L. Chen, Reciprocal regulation between support defects and strong metal-support interactions for highly efficient reverse water gas shift reaction over Pt/TiO_2 nanosheets catalysts, Appl. Catal., B, 298 (2021) 120507.

[28] J. Fang, Q. Chen, Z. Li, J. Mao, Y. Li, The synthesis of single-atom catalysts for heterogeneous catalysis, Chem. Commun., 59 (2023) 2854-2868.

[29] Y. Liu, Y. Sun, E. Zhao, W. Yang, J. Lin, Q. Zhong, H. Qi, A. Deng, S. Yang, H. Zhang, H. He, S. Liu, Z. Chen, S. Wang, Atomically Dispersed Silver- Cobalt Dual-Metal Sites Synergistically Promoting Photocatalytic Hydrogen Evolution, Adv. Funct.

Mater., 33 (2023) 2301840.

[30] T.W. van Deelen, C. Hernández Mejía, K.P. de Jong, Control of metal-support interactions in heterogeneous catalysts to enhance activity and selectivity, Nat. Catal., 2 (2019) 955-970.

[31] B. Lu, L. Guo, F. Wu, Y. Peng, J.E. Lu, T.J. Smart, N. Wang, Y.Z. Finfrock, D. Morris, P. Zhang, N. Li, P. Gao, Y. Ping, S. Chen, Ruthenium atomically dispersed in carbon outperforms platinum toward hydrogen evolution in alkaline media, Nat. Commun., 10 (2019) 631.

[32] X. Ning, Y. Li, B. Dong, H. Wang, H. Yu, F. Peng, Y. Yang, Electron transfer dependent catalysis of Pt on N-doped carbon nanotubes: Effects of synthesis method on metal-support interaction, J. Catal., 348 (2017) 100-109.

[33] X. Li, B.Y. Guan, S. Gao, X.W. Lou, A general dual-templating approach to biomass-derived hierarchically porous heteroatom-doped carbon materials for enhanced electrocatalytic oxygen reduction, Energy Environ. Sci., 12 (2019) 648-655.

[34] G. Li, J. Yu, J. Jia, L. Yang, L. Zhao, W. Zhou, H. Liu, Cobalt-Cobalt Phosphide Nanoparticles@Nitrogen-Phosphorus Doped Carbon/Graphene Derived from Cobalt Ions Adsorbed Saccharomycete Yeasts as an Efficient, Stable, and Large-Current-Density Electrode for Hydrogen Evolution Reactions, Adv. Funct. Mater., 28 (2018) 1801332.

[35] J.N. Tiwari, N.K. Dang, S. Sultan, P. Thangavel, H.Y. Jeong, K.S. Kim, Multi-heteroatom-doped carbon from waste-yeast biomass for sustained water splitting, Nat. Sustain., 3 (2020) 556-563.

[36] L. Zeng, A.R. Thiruppathi, J.v.d. Zalm, X. Li, A. Chen, Biomass-derived amorphous carbon with localized active graphite defects for effective electrocatalytic N_2 reduction, Appl. Surf. Sci., 575 (2022) 151630.

[37] J. Ma, Z. Yao, T.K.A. Hoang, Y. Liu, A. Sun, The intriguing ORR performance of iron and nitrogen co-doped biomass carbon composites incorporating surface-modified polyaniline-derived carbon, Fuel, 317 (2022) 123496.

[38] K. An, X. Xu, X. Liu, Mo2C-Based Electrocatalyst with Biomass-Derived Sulfur and Nitrogen Co-Doped Carbon as a Matrix for Hydrogen Evolution and Organic Pollutant Removal, ACS Sustainable Chem. Eng., 6 (2017) 1446-1455.

[39] H. Li, W. Ma, X. Ma, M. Guo, G. Li, Multifunctional Salt-Assisted Construction of Lignin-Derived Ru–Co Bimetal/Carbon Composites with Rich Nanointerface for Electrocatalytic Water Splitting, ACS Sustainable Chem. Eng., 10 (2022) 16214-16224.

[40] E. Ma, T. Shen, D. Ying, W. Liu, X. Zhao, L. Zhang, D. Wang, Chitin Derived Carbon Anchored Ultrafine Ru Nanoparticles for Efficient Hydrogen Evolution Reaction, ACS Sustainable Chem. Eng., 10 (2022) 15530-15537.

[41] L. Zeng, X. Li, S. Fan, J. Mu, M. Qin, X. Wang, G. Gan, M. Tadé, S. Liu, Seaweed-Derived Nitrogen-Rich Porous Biomass Carbon as Bifunctional Materials for Effective Electrocatalytic Oxygen Reduction and High-Performance Gaseous Toluene Absorbent, ACS Sustainable Chem. Eng., 7 (2019) 5057-5064.

[42] C. Durante, Metal–carbon interaction in metal nanoparticles and implication in the electrocatalysis of oxygen reduction, Curr. Opin. Electrochem, 36 (2022) 101119.

[43] K. Khan, X. Yan, Q. Yu, S.-H. Bae, J.J. White, J. Liu, T. Liu, C. Sun, J. Kim, H.-

M. Cheng, Y. Wang, B. Liu, K. Amine, X. Pan, Z. Luo, Stone-Wales defect-rich carbon-supported dual-metal single atom sites for Zn-air batteries, Nano Energy, 90 (2021) 106488.

[44] Y. Xie, Y. Chen, L. Liu, P. Tao, M. Fan, N. Xu, X. Shen, C. Yan, Ultra-High Pyridinic N-Doped Porous Carbon Monolith Enabling High-Capacity K-Ion Battery Anodes for Both Half-Cell and Full-Cell Applications, Adv. Mater., 29 (2017) 1702268.

[45] X.R. Wang, J.Y. Liu, Z.W. Liu, W.C. Wang, J. Luo, X.P. Han, X.W. Du, S.Z. Qiao, J. Yang, Identifying the Key Role of Pyridinic-N-Co Bonding in Synergistic Electrocatalysis for Reversible ORR/OER, Adv. Mater., 30 (2018) e1800005.

[46] Q. Wang, R. Yu, D. Shen, Q. Liu, K. Hong Luo, C. Wu, S. Gu, Performance of intrinsic heteroatoms in cobalt phosphide loaded ginkgo leave-based carbon material on promoting the electrocatalytic activity during hydrogen evolution reaction and oxygen evolution reaction, Fuel, 333 (2023) 126368.

[47] Y. Gong, D. Li, C. Luo, Q. Fu, C. Pan, Highly porous graphitic biomass carbon as advanced electrode materials for supercapacitors, Green Chem., 19 (2017) 4132-4140.

[48] X. Zhang, B. Sun, X. Fan, P. Liang, G. Zhao, B.K. Saikia, X. Wei, Hierarchical porous carbon derived from coal and biomass for high performance supercapacitors, Fuel, 311 (2022) 122552.

[49] J. Lei, K. Wang, B. Deng, Y. Li, S. Zhang, Y. Cao, Enhanced oxygen reduction of porous N-doped carbon nanosheets with graphitic N and defects obtained from coal-based graphene quantum dots, J. Alloys Compd., 914 (2022) 165359.

[50] W. Yu, H. Huang, Y. Qin, D. Zhang, Y. Zhang, K. Liu, Y. Zhang, J. Lai, L. Wang,

The Synergistic Effect of Pyrrolic- N and Pyridinic- N with Pt Under Strong Metal-Support Interaction to Achieve High- Performance Alkaline Hydrogen Evolution, Adv. Energy Mater., 12 (2022) 2200110.

[51] X. Dong, H. Yan, Y. Jiao, D. Guo, A. Wu, G. Yang, X. Shi, C. Tian, H. Fu, 3D hierarchical V–Ni-based nitride heterostructure as a highly efficient pH-universal electrocatalyst for the hydrogen evolution reaction, J. Mater. Chem. A, 7 (2019) 15823-15830.

[52] H. Yan, C. Tian, L. Wang, A. Wu, M. Meng, L. Zhao, H. Fu, Phosphorus-modified tungsten nitride/reduced graphene oxide as a high-performance, non-noble-metal electrocatalyst for the hydrogen evolution reaction, Angew Chem. Int. Ed., 54 (2015) 6325-6329.

[53] Q. Liu, J. Tian, W. Cui, P. Jiang, N. Cheng, A.M. Asiri, X. Sun, Carbon nanotubes decorated with CoP nanocrystals: a highly active non-noble-metal nanohybrid electrocatalyst for hydrogen evolution, Angew Chem. Int. Ed., 53 (2014) 6710-6714.

[54] H. Yan, Y. Xie, A. Wu, Z. Cai, L. Wang, C. Tian, X. Zhang, H. Fu, Anion-Modulated HER and OER Activities of 3D Ni-V-Based Interstitial Compound Heterojunctions for High-Efficiency and Stable Overall Water Splitting, Adv. Mater., 31 (2019) e1901174.

[55] S. Zhou, H. Jang, Q. Qin, L. Hou, M.G. Kim, S. Liu, X. Liu, J. Cho, Boosting Hydrogen Evolution Reaction by Phase Engineering and Phosphorus Doping on Ru/P-$TiO_{(2)}$, Angew Chem. Int. Ed., 61 (2022) e202212196.

[56] K. Wang, S. Wang, K.S. Hui, J. Li, C. Zha, D.A. Dinh, Z. Shao, B. Yan, Z. Tang,

K.N. Hui, Dense Platinum/Nickel Oxide Heterointerfaces with Abundant Oxygen Vacancies Enable Ampere- Level Current Density Ultrastable Hydrogen Evolution in Alkaline, Adv. Funct. Mater., 33 (2022) 2211273.

Declaration of interests

☒ The authors declare that they have no known competing financial interests or personal relationships that could have appeared to influence the work reported in this paper.

☐The authors declare the following financial interests/personal relationships which may be considered as potential competing interests: